RSC Advances

PAPER

Cite this: *RSC Adv.*, 2025, **15**, 44486

Adsorption of carbamazepine on self-endowed magnetic biochar produced from iron-rich sludge

Yan Liu,[a] Qianqian Li,[c] Honghui Pan,[a] Liying Liang,*[a] Liyang Zhao,*[ab] Qin Shi,[a] Chuanqi Zhao[a] and Xixiang Liu*[a]

Received 22nd May 2025
Accepted 3rd November 2025

DOI: 10.1039/d5ra03580e

rsc.li/rsc-advances

The preparation of magnetic biochar usually requires additives and additional synthesis steps, which leads to a significant increase in preparation costs. In this study, self-endowed magnetic biochar derived from iron-rich sludge was prepared *via* one-step pyrolysis to adsorb carbamazepine in water. The results show that when the initial concentration of carbamazepine is 5 mg L^{-1} and the dosage of self-endowed magnetic biochar is 0.9 g L^{-1}, the removal efficiency of carbamazepine by self-endowed magnetic biochar can reach 90.1%, and the adsorption performance is excellent in a wide pH range. The adsorption of carbamazepine by self-endowed magnetic biochar can be well fitted by Langmuir an adsorption isotherm and pseudo-second-order adsorption kinetic model, which indicates that the adsorption process is single molecular layer chemisorption. In addition, self-endowed magnetic biochar has good magnetic properties, and can be effectively separated and recovered by an external magnetic field after use, and the adsorption rate of carbamazepine can still reach 81.4% after repeated use for 5 times. The adsorption mechanism of carbamazepine by self-endowed magnetic biochar includes pore filling, complexation, $\pi-\pi$ interaction and hydrogen bonding.

Introduction

Pharmaceuticals are widely used to prevent and treat human and animal diseases. According to statistics, the global per capita annual consumption of pharmaceuticals is approximately 15 g, reaching as high as 50–150 g in industrialized countries.[1] Among them, carbamazepine (CBZ) as a typical drug is widely used in the treatment of seizures and neuralgia, the annual consumption has exceeded 1000 *t*, and the rate of release to water bodies is about 30 *t* per year.[2] Due to its strong hydrophilicity and resistance to biodegradation at low concentrations, CBZ can exist stably in aquatic environments.[3] It is one of the most frequently detected pharmaceuticals worldwide, even in the raw water sources of drinking water treatment plants.[4,5] However, long-term ingestion of CBZ may lead to decreased platelet, granulocyte, and leukocyte counts, and even hepatic and renal function failure, posing a serious threat to human health and ecosystem safety.[3] Therefore, it is crucial to develop an efficient, effective, and economical method for the removal of CBZ from aquatic environments.

Currently, the methods for removing CBZ from aquatic environments include membrane separation,[6] advanced oxidation processes,[7] electrochemical treatment[8] and adsorption.[9] Compared to the above-mentioned technologies, adsorption is considered to be the most promising method for the CBZ removal based on its high efficiency, simple operation, cost and practicality.[10] Numerous adsorbents have been produced and utilized for the removal of CBZ, including activated carbon,[11] silica-based materials,[12] chitosan-based materials[13] and biochar.[2] Among them, biochar is an ideal biomass adsorbent due to its abundant raw materials, low cost and environmental friendliness.[14,15] The main raw materials for the preparation of biochar include agricultural[16] and forestry wastes,[17] wood,[18] livestock manure[19] and sludge.[20] Nevertheless, cost considerations of raw materials have limited the widespread application of biochar for adsorption of pollutants. Therefore, it is significant to find the value-added materials as raw materials for biochar production. Sludge is a by-product of water treatment, and it is estimated that China's annual sludge production will exceed 90 million tons in 2025.[21] Owing to its low cost and high organic content, sludge is an ideal value-added material for biochar. Recently, sludge-based biochar has been widely used in the removal of heavy metals, dyes, phenols, inorganic salts and various pollutants.[22–24]

However, separating biochar from solid–liquid mixtures is challenging. Traditional separation processes such as coagulation, filtration, and sedimentation are inefficient and costly, limiting practical applications.[25] Magnetic biochar is prepared

[a]Guangxi Colleges and Universities Key Laboratory of Environmental-friendly Materials and New Technology for Carbon Neutralization, Guangxi Key Laboratory of Advanced Structural Materials and Carbon Neutralization, School of Materials and Environment, Guangxi Minzu University, Nanning 530006, China. E-mail: 20210011@gxmzu.edu.cn; 240946929@qq.com; liuxx200208@163.com
[b]College of New Energy and Environment, Jilin University, Changchun, 130021, China
[c]Huahong Water Group Co. Ltd, Nanning 530000, China

by loading magnetic materials such as iron, cobalt and nickel, which retains the excellent adsorption properties of biochar and overcomes the separation challenges of the materials.[26] However, the preparation of magnetic biochar typically involves additives and additional synthetic steps, the high cost and complicated process greatly limit the practical application of magnetic biochar. On the other hand, there are a large quantities of iron-rich sludges produced in wastewater plants because iron salts are widely used as flocculants and conditioners in wastewater treatment industries and sludge dewatering processes,[27] such as coagulation, phosphorus recovery, sulfide control and Fenton process. In the pyrolysis process of iron-rich iron sludge, biomass decomposes into reducing gases such as H_2, CO and CH_4 in an inert atmosphere,[28] which can reduce Fe_2O_3 in iron-rich sludge to Fe_3O_4 or even zero-valent iron.[29] Therefore, it is rational to hypothesize that self-endowed magnetic biochar can be produced from iron-rich sludge directly.

In this study, self-endowed magnetic sludge biochar was prepared by pyrolysis of iron-rich sludge in an inert atmosphere. CBZ was selected as the target pollutant, and the structure and properties of biochar was characterized by scanning electron microscopy (SEM), specific surface area and porosity analyzer (BET), organic element analyzer (EA), and X-ray photoelectron spectrometer (XPS). The adsorption kinetics, adsorption isotherm and characterization results before and after adsorption were investigated. The mechanism of CBZ adsorption by self-endowed magnetic sludge biochar was systematically revealed. This study aims to develop a low-cost method of magnetic biochar preparation for treating pharmaceutical wastewater and provide a new strategy for the resource utilization of iron-rich sludge.

Materials and methods

Reagents and materials

The iron-rich sludge was obtained from Guangxi Huahong Mingyang Industrial Wastewater Treatment Co.,Ltd located in Mingyang Industrial Park, Nanning City, and also treated iron salt wastewater generate from energy storage plants in addition to treating general industrial wastewater. The sewage treatment plant used the A^2/O process to treat industrial wastewater from the park. The metal oxide content of the iron-rich sludge listed in Table S1. The heavy metal level of the iron-rich sludge listed in Table S2. Anhydrous ethanol (C_2H_6O) and carbamazepine ($C_{15}H_{12}N_2O$) were procured from Shanghai McLennan Biochemical Technology Co., Ltd. Sodium hydroxide (NaOH) was purchased from Chengdu Jinshan Chemical Reagent Co., Ltd. Hydrochloric acid (HCl) was obtained from Shanghai Wokey Biotechnology Co., Ltd. All chemical reagents and drugs used in this study were used as received without further purification. Ultra-pure water was used for all experiments.

Preparation of magnetic sludge biochar

The iron-rich sludge was dried to constant weight and passed through a 100-mesh sieve, and 5 g was put into a corunjade boat, and then placed in a vacuum tube furnace (SK-G10123K, Tianjin Zhongyuan Electric Furnace Co., Ltd) for pyrolysis and carbonization under 0.1 L min^{-1} N_2 atmosphere. The heat treatment procedure was set as follows: the initial temperature was 25 °C, the target temperature was 300, 500, 700 and 900 °C respectively, and the rise rate of temperature was 5 °C min^{-1}. After reaching the target temperature, it was kept constant for 2 h, cooled to room temperature, cleaned repeatedly with ultra-pure water until the solution was colorless, and FBC_T samples were prepared after drying and sifting (T = 300–900 °C).

Characterization

Refer to the SI materials for the characterization of biochar (Text S1).

Adsorption experiments

Firstly, the adsorption performance of FBC at different pyrolysis temperatures for CBZ were investigated. In a typical test, 90 mg of FBC_T (T = 300–900) and 100 mL of 5 mg L^{-1} CBZ solution were added to 250 mL glass bottles successively, and the resulting mixture was shaken in a constant temperature oscillator at a rate of 200 r·min^{-1} for 4 h. A syringe was used to sample 0.5 mL of mixture, filtered through a 0.22 μm filter, and quantitative analysis was performed by high performance liquid chromatograph (LC-16, Shimadzu Company, Japan) equipped with a UV detector and an Inter Sustain C18 column (4.6 × 250 mm). The specific conditions for chromatographic analysis are as follows: the column temperature maintained at 35 °C, the mobile phase consisting of water and acetonitrile (volume ratio of 20 : 80), the flow rate was 1 mL min^{-1}, and the detection wavelength was set at 286 nm.

In the batch adsorption experiment, the effects of adsorbent dosage (0.1–1.3 g L^{-1}) and pH value (3–11) on the adsorption performance of FBC_{900} for CBZ were investigated. The adsorption capacity q (mg g^{-1}) and removal efficiency R (%) were used to evaluate the adsorption performance of FBC_{900} for CBZ. The calculation formulas for q_t and R are shown in eqn (1) and (2):

$$q_t = \frac{(C_0 - C_t)V}{m} \tag{1}$$

$$R = \frac{C_0 - C_t}{C_0} \times 100\% \tag{2}$$

where C_0 (mg L^{-1}) and C_t (mg L^{-1}) are the concentrations of CBZ at initial and time t, V (L) is the initial solution volume, m (g) is the adsorbent dose.

Adsorption kinetics

The experiment was conducted by dispersing 90 mg of FBC_{900} in 100 mL of 5 mg L^{-1} CBZ solution. The resulting mixture was oscillated for adsorption at a constant temperature of 25 °C in a constant temperature oscillator at a speed of 200 r·min^{-1}. Samples were taken at predetermined time intervals from 0 to 4 hours, and the remaining concentration of CBZ was measured and calculated. Two sets of parallel experiments were performed. The experimental results were analyzed and fitted using pseudo-first-order kinetics and pseudo-second-order kinetics models, represented by eqn (3) and (4) respectively:

$$\ln(q_e - q_t) = \ln q_e - k_1 t \tag{3}$$

$$\frac{t}{q_t} = \frac{1}{k_2 {q_e}^2} + \frac{t}{q_e} \tag{4}$$

where q_e and q_t represent the adsorption capacity at equilibrium and time t respectively (mg L^{-1}); t is the adsorption time (h); k_1 and k_2 are the pseudo-first-order kinetic rate constants (h^{-1}) and pseudo-second-order kinetic rate constants (g·[mg $h^{-1}]^{-1}$), respectively.

Adsorption isotherm

In 250 mL glass bottles, 90 mg of FBC_{900} and 100 mL of CBZ solution (5–130 mg L^{-1}) were added successively and adsorbed in a constant temperature oscillator at 25 °C for 4 h, respectively. Two parallel experiments were set up. Langmuir and Freundlich models were used for linear fitting of the experimental results, and the model formulas were shown in eqn (5) and (6) respectively:

$$\frac{C_e}{q_e} = \frac{C_e}{q_{max}} + \frac{1}{q_{max} k_L} \tag{5}$$

$$\ln q_e = \ln k_F + \frac{1}{n} \ln C_e \tag{6}$$

where C_e represents the concentration of CBZ at adsorption equilibrium (mg L^{-1}); q_e and q_{max} are the equilibrium adsorption capacity and the maximum theoretical adsorption capacity (mg g^{-1}), respectively. k_L and k_F represent Langmuir and Freundlich constants respectively. n is an empirical constant.

Regeneration and recycling of adsorbent

The FBC_{900}, after adsorbing CBZ, was isolated using a magnet, and the supernatant was decanted. It was then washed three times with methanol, repeating the magnetic separation and decantation process after each wash, followed by three washes with deionized water to ensure complete desorption. The desorbed mixture was then separated by applying a strong neodymium magnet with a magnetic field strength of 0.5 T for 10 min and dried in a constant temperature oven at 65 °C for later use. In order to test its regeneration performance, the adsorption performance of the regenerated FBC_{900} on CBZ was tested as follows: 90 mg of regenerated biochar was dispersed in 5 mg L^{-1} CBZ solution for shock adsorption for 4 h, and the remaining concentration of the filtrate was measured. Under the same experimental conditions, the adsorption and regeneration cycles were carried out five times.

Adsorption of different pharmaceuticals

Ibuprofen (IBP), tetracycline (TC), oxytetracycline hydrochloride (OTH), levofloxacin (LEV), and diclofenac (DCF) were used to investigate the adsorption properties of FBC_{900} to other contaminants. Specific as follows: 90 mg FBC_{900} was added to 100 mL of IBP, CBZ, OTH, LEV and DCF solutions with different concentrations, and the resulting mixture was adsorbed in a constant temperature oscillator at the rate of 200 r·min^{-1}. After reaching adsorption equilibrium, the residual concentration of pharmaceuticals was measured to explore the adsorption performance for the different pharmaceuticals.

Results and discussion

Characterization of FBC samples

The surface morphology of biochar samples was analyzed by scanning electron microscopy (SEM). As shown in Fig. 1, the morphology evolves significantly with pyrolysis temperature. The FBC_{300} sample exhibits a relatively smooth surface with large, flat, plate-like structures and minimal porosity. FBC_{500} shows a similar but slightly more eroded structure with the initial formation of some cavities. In stark contrast, FBC_{700} and FBC_{900} have significantly rough and loose porous surfaces. It can be found that with the gradual increase of pyrolysis temperature, the surface of biochar sample becomes rougher and the porosity also shows a gradual increase, a transformation attributed to the more intense volatilization and carbonization processes at higher temperatures. The rough and porous structure can increase the specific surface area of biochar and increase the surface adsorption sites.

To further investigate the specific surface area and pore structure characteristics of the samples, nitrogen adsorption–desorption isotherms (BET) tests were conducted on the FBC samples. As shown in Table 1, when the pyrolysis temperature of FBC increased, the average pore size of samples was 24.25, 17.07, 13.58 and 8.58 nm, respectively, all of which are mesoporous structures. With the increase of pyrolysis temperature, the specific surface area of the sample increased from 4.36 m^2 g^{-1} in FBC_{300} to 57.28 m^2 g^{-1} in FBC_{900}, the total pore volume increased from 0.05 cm^3 g^{-1} to 0.16 cm^3 g^{-1}, but the pore size decreased from 24.25 to 8.58 nm. This indicates that more micropores are formed during the thermal transformation process, and the development of this porous structure may lead to the increase of specific surface area.[30]

In order to further analyze the elemental composition of biochar samples, organic element analysis of FBC was carried out, and the analysis results are listed in Table 2. The C, H and O elements in biochar constitute its carbon skeleton and form functional groups, in which the H/C ratio reflects its aromaticity and carbonization degree, and the smaller the ratio, the stronger the aromaticity.[31] The O/C ratio is related to the hydrophilicity of biochar, and the lower the ratio, the weaker the hydrophilicity.[32] (O + N)/C indicates the polarity of the biochar, and a smaller ratio indicates a lower polarity.[33] As indicated in Table 2, with the increase in pyrolysis temperature, the H/C ratio of FBC continuously decreases. This is attributed to the thermal conversion of organic components into aromatic ring and other carbonized structures, indicating that the aromaticity and stability of FBC increase with the rise in pyrolysis temperature. The enhancement in aromaticity can strengthen the π–π interactions between the biochar in wastewater and pollutants.[34] The change in the O/C ratio with pyrolysis temperature is relatively small, indicating a weak

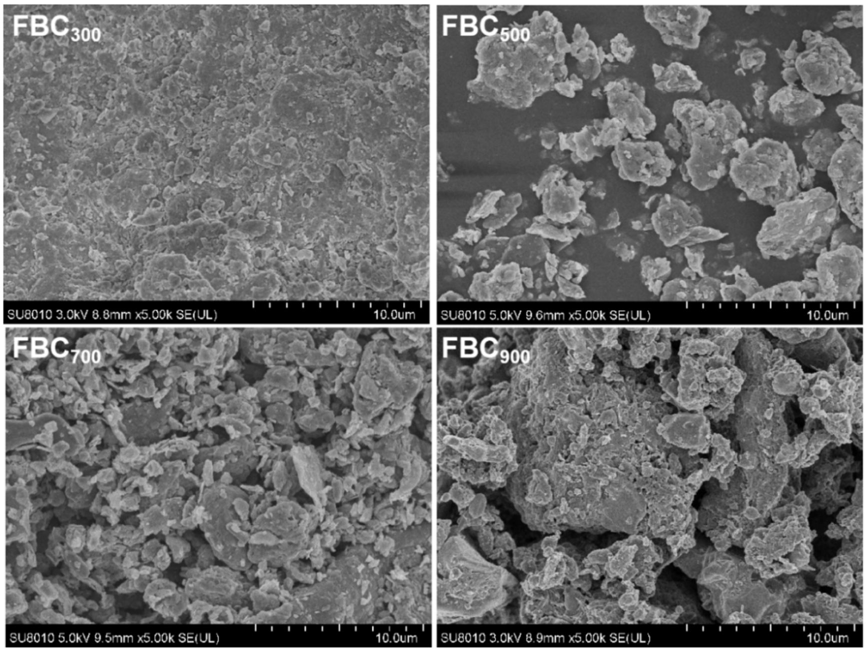

Fig. 1 SEM spectrum of FBC sample.

Table 1 Specific surface area and pore structure parameters of FBC samples

Sample	Specific surface area (m^2 g^{-1})	Pore volume (cm^3 g^{-1})	Pore size (nm)
FBC_{300}	4.36	0.05	24.25
FBC_{500}	25.01	0.09	17.07
FBC_{700}	40.45	0.14	13.58
FBC_{900}	57.28	0.16	8.58

Table 2 Elemental composition analysis of FBC samples

	C	H	O	N	H/C	O/C	(O + N)/C
Sample	wt%				Atomic ratio		
FBC_{300}	14.61	1.92	10.68	2.60	1.57	0.55	0.70
FBC_{500}	10.16	0.95	7.89	1.58	1.36	0.71	0.87
FBC_{700}	9.77	0.49	6.52	1.00	0.60	0.50	0.59
FBC_{900}	5.61	0.18	4.12	0.23	0.39	0.55	0.58

variation in its hydrophilic properties. However, the (O + N)/C atomic ratio continuously decreases with the increase in pyrolysis temperature, indicating the continuous decomposition of polar functional groups in FBC.

The surface chemical composition of FBC samples was analyzed by XPS. As shown in Fig. 2, three characteristic peaks were observed at 288.6, 286.2, and 284.8 eV of the C1S XPS spectrum (Fig. 2a), corresponding to C=O, C–O, and C–C/C=C, respectively. By calculating the proportion of peak area of C–O and C=O (Table S3), it is observed that with the increase of pyrolysis temperature, the proportion of C–O shows an increasing trend (14.8 → 22.2 → 22.7 → 36.7%), while the proportion of C=O shows a decreasing trend (14.8 → 11.2 → 10.6 → 5.2%). In addition, high-resolution Fe 2p XPS spectra show characteristic peaks for Fe(III) (713.4 and 726.6 eV) and Fe(II) (711.1 eV and 724.2 eV) species, along with their satellite peaks (labeled as 'sat'). As shown in Table S2, the relative proportions of Fe(III) and Fe(II) in FBC_{300} are 58.9% and 41.1%, respectively. With the increase of pyrolysis temperature, the content of Fe(II) increases gradually, and the maximum relative proportion of Fe(II) in FBC_{900} increases to 62.8%. In general, high-valence iron is reduced to low-valence iron (Fe_2O_3 → Fe_3O_4) by reaction with organic molecules and the fission products of biological macromolecules (reducing substances such as C, CO, and CH_4) during anaerobic pyrolysis.[35] Therefore, with the continuous rise of pyrolysis temperature, iron oxide is gradually transformed from Fe_2O_3 to Fe_3O_4.

As shown in Fig. 3, the magnetic properties of the FBC samples were analyzed using a vibrating sample magnetometer (VSM). The magnetization curves show that all biochars exhibit ferromagnetic behavior. The saturation magnetization (M_s) value, read from the vertical axis at the highest applied field (horizontal axis, Applied Magnetic Field), increases progressively with pyrolysis temperature. The results show that with the increase of pyrolysis temperature, the saturation magnetic susceptibility of FBC increases gradually, and the magnetic susceptibility of FBC_{900} is the highest, reaching 0.85emu g^{-1}. As a result, FBC samples can be recovered by magnetic separation, overcoming the high cost problems caused by traditional separation techniques such as coagulation, precipitation, and filtration. With increasing pyrolysis temperature, the original Fe_2O_3 in iron-rich sludge transforms into Fe_3O_4. Theoretically, without the need for any additives, iron-rich sludge can be

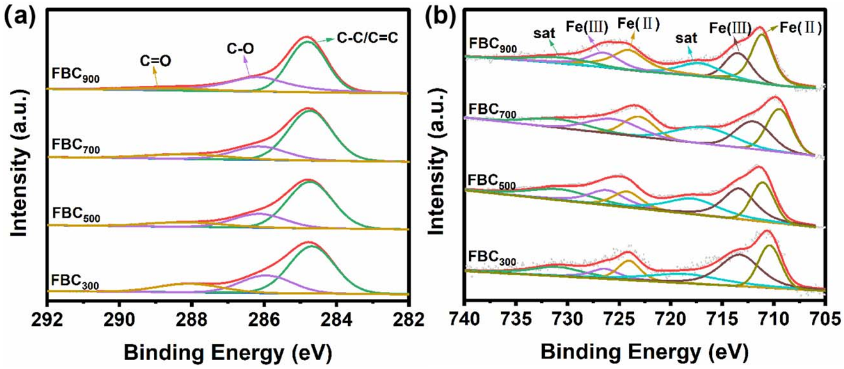

Fig. 2 High-resolution XPS spectra of FBC samples: (a) C 1s and (b) Fe 2p spectra.

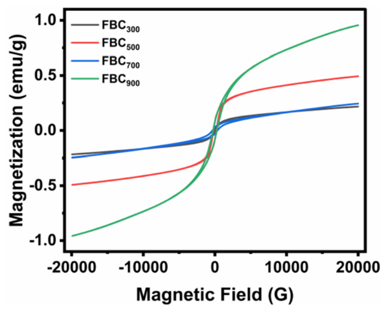

Fig. 3 Magnetic hysteresis loops of FBC samples measured by VSM.

pyrolyzed under anaerobic conditions to produce magnetic biochar.

Adsorption properties of FBC for CBZ

The adsorption performance of FBC at different pyrolysis temperatures on CBZ is depicted in Fig. 4. As the pyrolysis temperature increased 300 °C to 900 °C, the removal efficiency of CBZ by FBC increased from 7.5% to 90.5% This enhancement is attributed to the increase in specific surface area and pore volume; higher surface area and a more abundant pore structure offer additional active sites, thereby augmenting the adsorption capacity of FBC for pollutants. Simultaneously, the adsorption results showed the adsorption capacities were remarkably superior to that of the pristine iron-rich sludge. Considering the temperature requirements for preparing biochar and its outstanding adsorption capacity, FBC_{900} was selected for subsequent adsorption studies.

The effect of different dosage of adsorbents on the adsorption of CBZ by FBC_{900} was shown in Fig. 5. With the increasing dosage of FBC900, the removal efficiency of CBZ also increased, because the increase of adsorbents provided more adsorption sites. Simultaneously, the adsorption capacity decreased from 6.4 to 4.5 mg g^{-1} with the dosage increasing from 0.1 to 1.3 g L^{-1}, indicating reduced utilization efficiency of adsorption sites at higher dosages. When the dosage of FBC_{900} was 0.9 g L^{-1}, the removal efficiency of CBZ can reach 90.5%, and then with the increased of the dosage of adsorbents, the removal efficiency of CBZ increased slowly. Therefore, 0.9 g L^{-1} was selected as the best dosage for subsequent adsorption experiments.

The pH value of the solution is a crucial factor in most of adsorption process. The effect of pH on the removal of CBZ from FBC_{900} was studied at different pH values (3, 5, 7, 9 and 11). As shown in Fig. 6a, the highest removal efficiency of 88.4% and adsorption capacities ranging from 3.9 to 4.4 mg g^{-1}. Was observed at pH 7. The As shown in Fig. 6a, the highest removal efficiency of 88.4% was observed at pH 7. The point of zero charge (pH_{PZC}) of FBC_{900} is 5.86 (Fig. 6b), indicating that the surface of FBC_{900} is positively charged when the solution pH < 5.86, and the surface of FBC_{900} is negatively charged when the

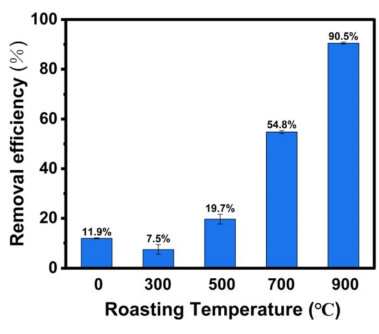

Fig. 4 Adsorption properties of FBC for CBZ. Experimental conditions:C_0 = 5 mg L^{-1}, m = 0.9 g L^{-1}, V = 100 mL, pH = 7; adsorbents: sludge, FBC_{300}, FBC_{500}, FBC_{700}, FBC_{900}.

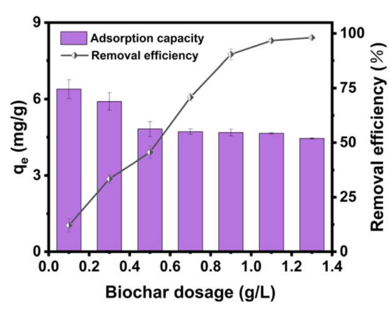

Fig. 5 Effect of FBC_{900} dosage on adsorption of CBZ. Experimental conditions: C_0 = 5 mg L^{-1}, m = 0.1–1.3 g L^{-1}, V = 100 mL and pH = 7.

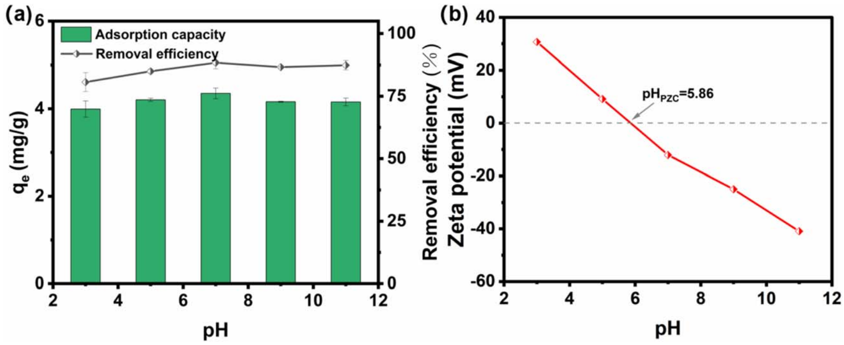

Fig. 6 Effect of solution pH on adsorption of CBZ by FBC (a) and Zeta potential of FBC (b). Experimental conditions: $C_0 = 5$ mg L^{-1}, $m = 0.9$ g L^{-1}, $V = 100$ mL and pH = 3–11.

solution pH > 5.86. However, the experimental results showed that regardless of the surface charge of FBC_{900}, CBZ can be adsorbed well in a wide pH range. In the pH range studied (3–11), the CBZ molecule remained neutral,[36] indicating a low electrostatic attraction with the charged FBC_{900} or was not controlled by electrostatic interactions.

Adsorption kinetics and isotherm

In order to further study the relationship between adsorbents, pollutants and adsorption time, adsorption kinetics experiments were conducted (Fig. 7), and pseudo-first-order and pseudo-second-order kinetic models were used to fit the adsorption experimental data. These models were selected because they are widely used in adsorption studies to distinguish between physical and chemical adsorption processes. Kinetic fitting parameters were shown in Table S4. The calculated values of pseudo-first-order kinetic equilibrium adsorption capacity were 2.62 mg g^{-1}, and the correlation coefficient R^2 of the fitting curve was 0.402. The calculated values of pseudo-second-order kinetic equilibrium adsorption capacity were 4.76 mg g^{-1}, respectively, and the correlation coefficient R^2 of the fitting curve was 0.999. The results showed that the calculated adsorption capacity was closer to the experimental value (4.79 mg g^{-1}) and had a higher correlation coefficient, indicating that the adsorption of CBZ by FBC_{900} was more consistent with the pseudo-second-order kinetics. The pseudo-second-order kinetics included adsorption processes such as liquid film diffusion, surface adsorption, in-particle diffusion, and electron sharing or transfer,[37] while the pseudo-first-order kinetics is generally only suitable for describing the initial stage of adsorption.[38] Therefore, the pseudo-second-order kinetic model can more reasonably describe the adsorption process, indicating that the adsorption of CBZ by FBC_{900} is mainly chemisorption.[39]

The adsorption capacity was explored when the adsorption reached equilibrium at 25 °C. The Langmuir model and Freundlich model were both used to fit the experimental data (Fig. 8), and the fitting parameters were shown in Table S5. The linear fitting correlation coefficient of Langmuir model(R^2) was 0.962, while that of Freundlich model was 0.919. The fitting effect of the Langmuir model was significantly better than that of the Freundlich model, and the calculated saturation adsorption value (18.83 mg g^{-1}) was closer to the experimental value (18.23 mg g^{-1}), indicating that the adsorption of CBZ by FBC_{900} was more consistent with the Langmuir model, and the adsorption is a single molecular layer adsorption on a uniform surface.[40,41]

Reusability

The reusability of adsorbent is an important index to evaluate the adsorption performance of adsorbent. The adsorbed FBC_{900} was separated from the wastewater, and the adsorption effect of

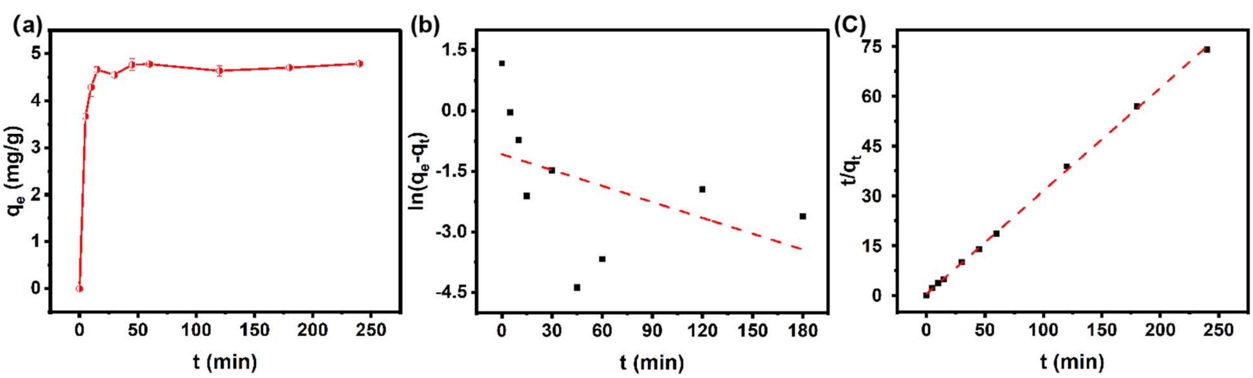

Fig. 7 (a) Adsorption kinetics of FBC_{900}. (b) Pseudo-first-order kinetic model. (c) Pseudo-second-order kinetic model.

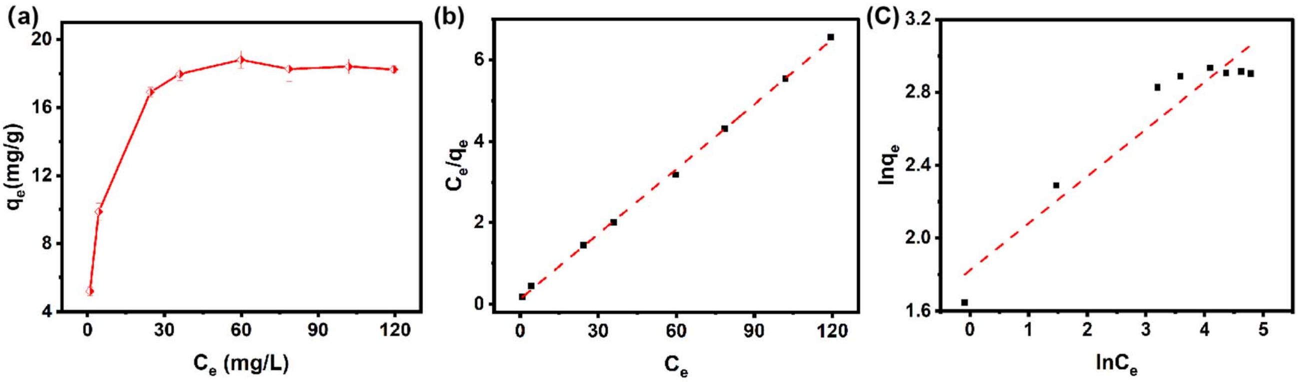

Fig. 8 (a) Adsorption isotherm of FBC_{900} (b) Langmuir isotherm (c) Freundlich isotherm. Experimental conditions: C_0(CBZ) = 5–30 mg L^{-1}, $m(FBC_{900})$ = 0.9 g L^{-1}, V = 100 mL and pH = 7.

five cycles were investigated. As shown in Fig. 9, the removal efficiency of CBZ was some reduction while the adsorption–desorption cycles of FBC_{900} increased,this may be due to the blockage of the pore structure of FBC_{900} and the reduction of binding sites.[34] In spite of this, the removal of CBZ by FBC_{900} was still able to exceed of 81.7%. In addition, leaching experiments were carried out on FBC_{900}. As shown in Table S6, the leaching of organic matter and heavy metals in the system was insignificant. These results indicateed that FBC_{900} has good stability and safety, and remained efficient for reuse even after multiple cycling experiments.

The adsorption of different pharmaceuticals

Through the aforementioned experimental studies, it was found that FBC_{900}, a biochar adsorbent prepared by pyrolysis of iron-rich sludge, can effectively remove CBZ from water bodies while enabling magnetic recovery and recycling. However, in order to investigate its universality for pollutants adsorption, the adsorption performance of FBC_{900} on other kinds of pharmaceuticals was investigated. As shown in Fig. 10, the removal rates of 3 mg L^{-1} IBP, 20 mg L^{-1} CBZ, 15 mg L^{-1} OTH, 10 mg L^{-1} LEV, and 10 mg L^{-1} DCF can reach over 90% when the dosage of FBC_{900} was 0.9 g L^{-1}, which fully demonstrated that it could effectively remove CBZ from the water body and achieve magnetic recovery and recycling at the same time. more than 90%, which fully demonstrated its excellent general applicability.

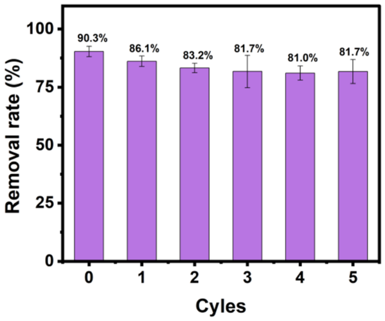

Fig. 9 The reusability of FBC_{900}. Experimental conditions: C_0 = 5 mg L^{-1}, m = 0.9 g L^{-1}, V = 100 mL and pH = 7.

Adsorption mechanism

In this study, according to the SEM image of the adsorption of CBZ by FBC_{900} (Fig. S1), it can be observed that the surface of the adsorbent material is covered with more uplift parts, showing an uneven structure. It is speculated that CBZ molecules may be adsorbed to the interior of the carbon material through pore filling and eventually aggregate on the surface. By comparing BET data before and after adsorption of CBZ by FBC_{900} (Table 2 and S7), it can be found that after adsorption, the specific surface area and pore volume of FBC_{900} decrease from 57.28 to 29.55 m^2 g^{-1}, and the pore volume decreases from 0.16 to 0.08 cm^3 g^{-1}, and both the specific surface area and total pore volume decrease. This indicates that CBZ is adsorbed to the surface and inside the pores of FBC_{900} through pore filling.

According to the infrared spectra before and after CBZ adsorption by FBC_{900} (Fig. 11), the Fe–O peak at 548 cm^{-1} of FBC_{900} was shifted by 563 cm^{-1} after adsorption, indicating that the presence of Fe–O may provide additional adsorption sites for complexation. The peaks of C=O, O=C–O, and C–H functional groups shifted to a certain extent, indicating that the π–π interaction between FBC_{900} and pollutant CBZ participated in the adsorption process.[36] The C–O and O–H stretching vibration peaks of FBC_{900} at 1060 and 3239 cm^{-1} migrated to 1075 and 3214 cm^{-1} after adsorption, indicating that oxygen-containing

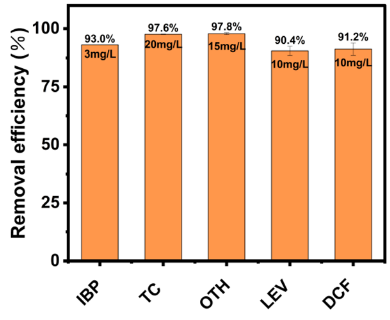

Fig. 10 The adsorption of different pharmaceuticals. Experimental conditions: C_0=(3 mg L^{-1} IBP, 20 mg L^{-1} CBZ, 15 mg L^{-1} OTH, 10 mg L^{-1} LEV, 10 mg L^{-1} DCF), m = 0.9 g L^{-1}, V = 100 mL and pH = 3–11.

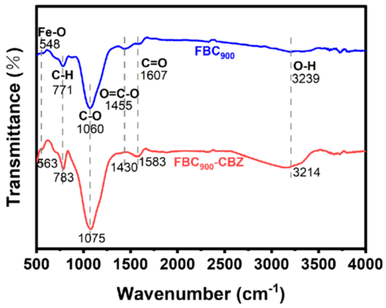

Fig. 11 Infrared spectra of FBC_{900} before and after adsorption of CBZ.

functional groups participated in CBZ binding through hydrogen bonding.[42] In summary, the adsorption of CBZ by FBC_{900} includes pore filling, complexation, π–π interaction and hydrogen bonding.

Conclusion

(1) Self-endowed magnetic biochar (FBC_{900}) was prepared by using iron-rich sludge as raw material at the pyrolysis temperature of 900 °C. When the initial concentration of CBZ was 5 mg L^{-1} and the dosage of FBC_{900} was 0.9 g L^{-1}, the removal efficiency of CBZ can reach 90.1%.

(2) The adsorption of CBZ by FBC_{900} conformed to the Langmuir adsorption isotherm and the pseudo-second-order adsorption kinetic model, and the adsorption process was single molecular layer chemisorption.

(3) FBC_{900} has good magnetic properties, which can be effectively separated and recovered by an external magnetic field after use. After repeated use for 5 times, the removal efficiency of CBZ can still reach 81.7%

(4) At the dosage of 0.9 g L^{-1} of FBC_{900}, the removal rates of 3 mg L^{-1} IBP, 20 mg L^{-1} CBZ, 15 mg L^{-1} OTH, 10 mg L^{-1} LEV, and 10 mg L^{-1} DCF reached more than 90%. It demonstrated that FBC_{900} had a excellent adsorption properties for different pharmaceuticals.

Conflicts of interest

The authors declare that they have no known competing financial interests or personal relationships that could have appeared to influence the work reported in this paper.

Data availability

The data supporting this article have been included as part of the supplementary information (SI). Supplementary information (SI) is available. See DOI: **https://doi.org/10.1039/d5ra03580e**.

Acknowledgements

This work was supported by the National Natural Science Foundation of China (No. 41967030), Guangxi Natural Science Foundation (2025GXNSFAA069248), Specific Research Project of Guangxi for Research Bases and Talents (AD23026173), the Young Scholar Innova tion Team of Guangxi Minzu University (2022) and Scientific Research Foundation for introduced Talents of Guangxi Minzu University (No. 2018KJQD08, 2022KJQD29 and 2022KJQD32).

References

1 Y. Zhang, S. U. Geissen and C. Gal, Carbamazepine and diclofenac: removal in wastewater treatment plants and occurrence in water bodies, *Chemosphere*, 2008, **73**(8), 1151–1161.
2 M. Naghdi, M. Taheran, R. Pulicharla, *et al.*, Pine-wood derived nanobiochar for removal of carbamazepine from aqueous media: Adsorption behavior and influential parameters, *Arabian J. Chem.*, 2019, **12**(8), 5292–5301.
3 D. Chen, S. Xie, C. Chen, *et al.*, Activated biochar derived from pomelo peel as a high-capacity sorbent for removal of carbamazepine from aqueous solution, *RSC Adv.*, 2017, **7**(87), 54969–54979.
4 A. Almeida, V. Calisto, V. I. Esteves, *et al.*, Presence of the pharmaceutical drug carbamazepine in coastal systems: effects on bivalves, *Aquat. Toxicol.*, 2014, **156**, 74–87.
5 A. Jelic, M. Gros, A. Ginebreda, *et al.*, Occurrence, partition and removal of pharmaceuticals in sewage water and sludge during wastewater treatment, *Water Res.*, 2011, **45**(3), 1165–1176.
6 M. Yao, L. Duan, J. Wei, *et al.*, Carbamazepine removal from wastewater and the degradation mechanism in a submerged forward osmotic membrane bioreactor, *Bioresour. Technol.*, 2020, **314**, 123732.
7 J. Im, I. Cho, S. Kim, *et al.*, Optimization of carbamazepine removal in $O_3/UV/H_2O_2$ system using a response surface methodology with central composite design, *Desalination*, 2012, **285**(31), 306–314.
8 F. Al-Qaim, Z. Mussa, A. Yuzir, *et al.*, Full Factorial Experimental Design for Carbamazepine Removal Using Electrochemical Process: a Case Study of Scheming the Pathway Degradation, *J. Braz. Chem. Soc.*, 2018, **29**(8), 1721–1731.
9 N. E. Al-Ghoul, G. A. Albarghouti and R. G. Qandeel, Activated carbon-based pomegranate peels as an efficient removal method for carbamazepine, *Environ. Monit. Assess.*, 2023, **195**(7), 821.
10 S. M. M. B. María Alejandra Décima, A Review on the Removal of Carbamazepine from Aqueous Solution by Using Activated Carbon and Biochar, *Sustainability*, 2021, (13), 11760.
11 X. Li, F. I. Hai and L. D. Nghiem, Simultaneous activated carbon adsorption within a membrane bioreactor for an enhanced micropollutant removal, *Bioresour. Technol.*, 2011, **102**(9), 5319–5324.
12 M. E. Peralta, D. O. Mártire, M. S. Moreno, *et al.*, Versatile nanoadsorbents based on magnetic mesostructured silica nanoparticles with tailored surface properties for organic pollutants removal, *J. Environ. Chem. Eng.*, 2021, **9**(1), 104841.

13 K. Fang, L. Deng, J. Yin, *et al.*, Recent advances in starch-based magnetic adsorbents for the removal of contaminants from wastewater: A review, *Int. J. Biol. Macromol.*, 2022, **218**, 909–929.
14 H. Liang, C. Zhu, S. Ji, *et al.*, Magnetic Fe_2O_3/biochar composite prepared in a molten salt medium for antibiotic removal in water, *Biochar*, 2022, **4**(1), 3.
15 Q. Zhang, H. Cai, W. Yi, *et al.*, Biocomposites from Organic Solid Wastes Derived Biochars: A Review, *Materials*, 2020, **13**(18), 3923.
16 M. Liang, L. Lu, H. He, *et al.*, Applications of Biochar and Modified Biochar in Heavy Metal Contaminated Soil: A Descriptive Review, *Sustainability*, 2021, **13**(24), 14041.
17 J. O. Eduah, E. K. Nartey, M. K. Abekoe, *et al.*, Phosphorus retention and availability in three contrasting soils amended with rice husk and corn cob biochar at varying pyrolysis temperatures, *Geoderma*, 2019, **341**, 10–17.
18 F. Debela, R. W. Thring and J. M. Arocena, Immobilization of Heavy Metals by Co-pyrolysis of Contaminated Soil with Woody Biomass, *Water, Air, Soil Pollut.*, 2012, **223**(3), 1161–1170.
19 C. H. Liu, Y. H. Chuang, H. Li, *et al.*, Sorption of Lincomycin by Manure-Derived Biochars from Water, *J. Environ. Qual.*, 2016, **45**(2), 519–527.
20 J. Zhang, J. Shao, Q. Jin, *et al.*, Sludge-based biochar activation to enhance Pb(II) adsorption, *Fuel*, 2019, **252**, 101–108.
21 H. Liu, H. Qiao, S. Liu, *et al.*, Energy, environment and economy assessment of sewage sludge incineration technologies in China, *Energy*, 2023, **264**, 126294.
22 P. Devi and A. K. Saroha, Utilization of sludge based adsorbents for the removal of various pollutants: A review, *Sci. Total Environ.*, 2017, **578**, 16–33.
23 H. Cheng, Y. Liu and X. Li, Adsorption performance and mechanism of iron-loaded biochar to methyl orange in the presence of Cr^{6+} from dye wastewater, *J. Hazard. Mater.*, 2021, **415**, 125749.
24 Y. Liu, H. Cheng and Y. He, Application and Mechanism of Sludge-Based Activated Carbon for Phenol and Cyanide Removal from Bio-Treated Effluent of Coking Wastewater, *Processes*, 2020, **8**(1), 82.
25 X. Li, C. Wang, J. Zhang, *et al.*, Preparation and application of magnetic biochar in water treatment: A critical review, *Sci. Total Environ.*, 2020, **711**, 134847.
26 Y. Yi, Z. Huang, B. Lu, *et al.*, Magnetic biochar for environmental remediation: A review, *Bioresour. Technol.*, 2020, **298**, 122468.
27 H. Luo, Y. Sun, M. Taylor, *et al.*, Impacts of aluminum- and iron-based coagulants on municipal sludge anaerobic digestibility, dewaterability, and odor emission, *Water Environ. Res.*, 2021, **94**(1), e1684.
28 L. Zhao, Y. Zhao, H. Nan, *et al.*, Suppressed formation of polycyclic aromatic hydrocarbons (PAHs) during pyrolytic production of Fe-enriched composite biochar, *J. Hazard. Mater.*, 2020, **382**, 121033.
29 N. Bombuwala Dewage, A. S. Liyanage, Q. Smith, *et al.*, Fast aniline and nitrobenzene remediation from water on magnetized and nonmagnetized Douglas fir biochar, *Chemosphere*, 2019, **225**, 943–953.
30 L. Wu, Y. Li, X. Kong, *et al.*, Mechanism evolution and prediction of carbamazepine sorption by mangrove plant residue–derived biochars, *J. Environ. Qual.*, 2022, **51**(4), 745–754.
31 J. Luo, J. Lin, R. Ma, *et al.*, Effect of different ash/organics and C/H/O ratios on characteristics and reaction mechanisms of sludge microwave pyrolysis to generate bio-fuels, *Waste Manage.*, 2020, **117**, 188–197.
32 B. Li, Y. Huang, Z. Wang, *et al.*, Enhanced adsorption capacity of tetracycline on tea waste biochar with KHCO3 activation from aqueous solution, *Environ. Sci. Pollut. Res.*, 2021, **28**(32), 44140–44151.
33 Z. Zhao, Q. Wu, T. Nie, *et al.*, Quantitative evaluation of relationships between adsorption and partition of atrazine in biochar-amended soils with biochar characteristics, *RSC Adv.*, 2019, **9**(8), 4162–4171.
34 Y. Mei, J. Xu, Y. Zhang, *et al.*, Effect of Fe–N modification on the properties of biochars and their adsorption behavior on tetracycline removal from aqueous solution, *Bioresour. Technol.*, 2021, **325**, 124732.
35 S. Tao, J. Yang, H. Hou, *et al.*, Enhanced sludge dewatering *via* homogeneous and heterogeneous Fenton reactions initiated by Fe-rich biochar derived from sludge, *Chem. Eng. J.*, 2019, **372**, 966–977.
36 G. Liang, Z. Hu, Z. Wang, *et al.*, Effective removal of carbamazepine and diclofenac by $CuO/Cu_2O/Cu$-biochar composite with different adsorption mechanisms, *Environ. Sci. Pollut. Res.*, 2020, **27**(36), 45435–45446.
37 S. Fan, J. Tang, Y. Wang, *et al.*, Biochar prepared from co-pyrolysis of municipal sewage sludge and tea waste for the adsorption of methylene blue from aqueous solutions: Kinetics, isotherm, thermodynamic and mechanism, *J. Mol. Liq.*, 2016, **220**, 432–441.
38 L. Qi, F. Teng, X. Deng, *et al.*, Experimental study on adsorption of Hg(II) with microwave-assisted alkali-modified fly ash, *Powder Technol.*, 2019, **351**, 153–158.
39 H. Yang, H. Yu, J. Wang, *et al.*, Magnetic porous biochar as a renewable and highly effective adsorbent for the removal of tetracycline hydrochloride in water, *Environ. Sci. Pollut. Res.*, 2021, **28**(43), 61513–61525.
40 S. Liu, J. Li, S. Xu, *et al.*, A modified method for enhancing adsorption capability of banana pseudostem biochar towards methylene blue at low temperature, *Bioresour. Technol.*, 2019, **282**, 48–55.
41 S. Fan, X. Fan, S. Wang, *et al.*, Effect of chitosan modification on the properties of magnetic porous biochar and its adsorption performance towards tetracycline and Cu^{2+}, *Sustainable Chem. Pharm.*, 2023, **33**, 101057.
42 K. Wang, R. Yao, D. Zhang, *et al.*, Tetracycline Adsorption Performance and Mechanism Using Calcium Hydroxide-Modified Biochars, *Toxics*, 2023, **11**(10), 841.

